Rotation of gap nodes in the topological superconductor $Cu_x(PbSe)_5(Bi_2Se_3)_6$

Mahasweta Bagchi [1], Jens Brede [1,*], Aline Ramires [2,†] and Yoichi Ando [1,‡]
[1]*Physics Institute II, University of Cologne, D-50937 Köln, Germany*
[2]*Paul Scherrer Institute, CH-5232 Villigen PSI, Switzerland*

(Received 12 October 2023; revised 22 December 2023; accepted 9 February 2024; published 15 March 2024)

Among the family of odd-parity topological superconductors derived from Bi_2Se_3, $Cu_x(PbSe)_5(Bi_2Se_3)_6$ (CPSBS) has been elucidated to have gap nodes. Although the nodal gap structure has been established by specific-heat and thermal-conductivity measurements, there has been no direct observation of the superconducting gap of CPSBS using scanning tunneling spectroscopy (STS). Here we report the first STS experiments on CPSBS down to 0.35 K, which found that the vortices generated by out-of-plane magnetic fields have an elliptical shape, reflecting the anisotropic gap structure. The orientation of the gap minima is found to be aligned with the bulk direction when the surface lattice image shows twofold symmetry, but, surprisingly, it is rotated by 30° when twofold symmetry is absent. In addition, the superconducting gap spectra in zero magnetic field suggest that the gap nodes are most likely lifted. We argue that only an emergent symmetry at the surface, allowing for a linear superposition of gap functions with different symmetries in the bulk, can lead to the rotation of the gap nodes. The absence of inversion symmetry at the surface additionally lifts the nodes. This result establishes the subtle but crucial role of crystalline symmetry in topological superconductivity.

DOI: 10.1103/PhysRevB.109.104507

I. INTRODUCTION

Topological superconductivity is a current hot topic in condensed matter physics due to its close relevance to Majorana fermions [1]. However, not many materials have been conclusively identified as topological superconductors. The family of bulk superconductors derived from Bi_2Se_3 presents a rare case, in which odd-parity topological superconductivity has been well established [1,2]. In this class of materials, despite the threefold rotational symmetry of the lattice, bulk superconducting (SC) properties consistently show peculiar twofold symmetry [3–9] that points to the realization of an odd-parity gap function with E_u symmetry. Although this gap function is unconventional and strongly anisotropic, the superconductivity is nonetheless protected from disorder due to the generalized Anderson's theorem, thanks to the additional orbital degrees of freedom and layered structure [10–12].

Interestingly, the E_u-symmetric gap function under D_{3d} symmetry, conventionally called Δ_4 [13,14], is generally a linear superposition of two basis functions, conventionally called Δ_{4x} and Δ_{4y}, which have nodes along a mirror plane of the crystal lattice or normal to it, respectively. The coefficients of the superposition form the nematic director **n** [14]. In the presence of a principal rotation axis with threefold symmetry, there are three degenerate superpositions of these basis functions, corresponding to three distinct nematic directors. The selection of one of these superpositions endows a nematic character to the SC state. Note that only the mirror-symmetry-protected nodes are expected to be robust under the D_{3d} symmetry, while others can be lifted by perturbations such as a warping term in the normal state electronic structure [14]. Elucidating the factors that dictate the nematic axis is important not only for understanding the topological superconductivity in the Bi_2Se_3-based compounds but also for finding ways to manipulate the SC gap [15].

Experimentally, the orientation of the gap minima differs among experiments even for the same compound [2]. For example, in $Cu_xBi_2Se_3$, the direction of the gap minima has been reported to be 90° rotated between bulk [4] and surface [16] measurements. In this regard, there is a complexity arising from the threefold rotational symmetry of the Bi_2Se_3 lattice, which allows for three equivalent rotational domains [2,4]; when contributions from two or more domains are superposed, the apparent symmetry may look like, e.g., Δ_{4x} even when the true symmetry is Δ_{4y} [4,17].

Fortunately, this complexity is absent in the superconductor $Cu_x(PbSe)_5(Bi_2Se_3)_6$ (hereafter called CPSBS) [9,11,18]. which has a monoclinic crystal structure and a topologically nontrivial twofold symmetric gap function [1,13,19]. Specifically, Andersen *et al.* [9] showed that the gap function in CPSBS has nodes located on the unique crystallographic mirror plane, giving rise to nodal superconductivity in the bulk, which was evinced by specific-heat [9] and thermal-conductivity [11] measurements in the mK regime. In this paper, we use scanning tunneling microscopy (STM) and spectroscopy (STS) to directly access the SC gap on the surface of CPSBS. On a relatively clean surface, we found that vortices generated under out-of-plane magnetic fields are elongated in a twofold-symmetric manner, and the elongation occurs in the direction perpendicular to the bulk gap nodes. This is contrary to the naive expectation that the coherence length should be longer along the direction of the gap nodes [16], but it is actually consistent with recent theoretical

*brede@ph2.uni-koeln.de
†aline.ramires@psi.ch
‡ando@ph2.uni-koeln.de

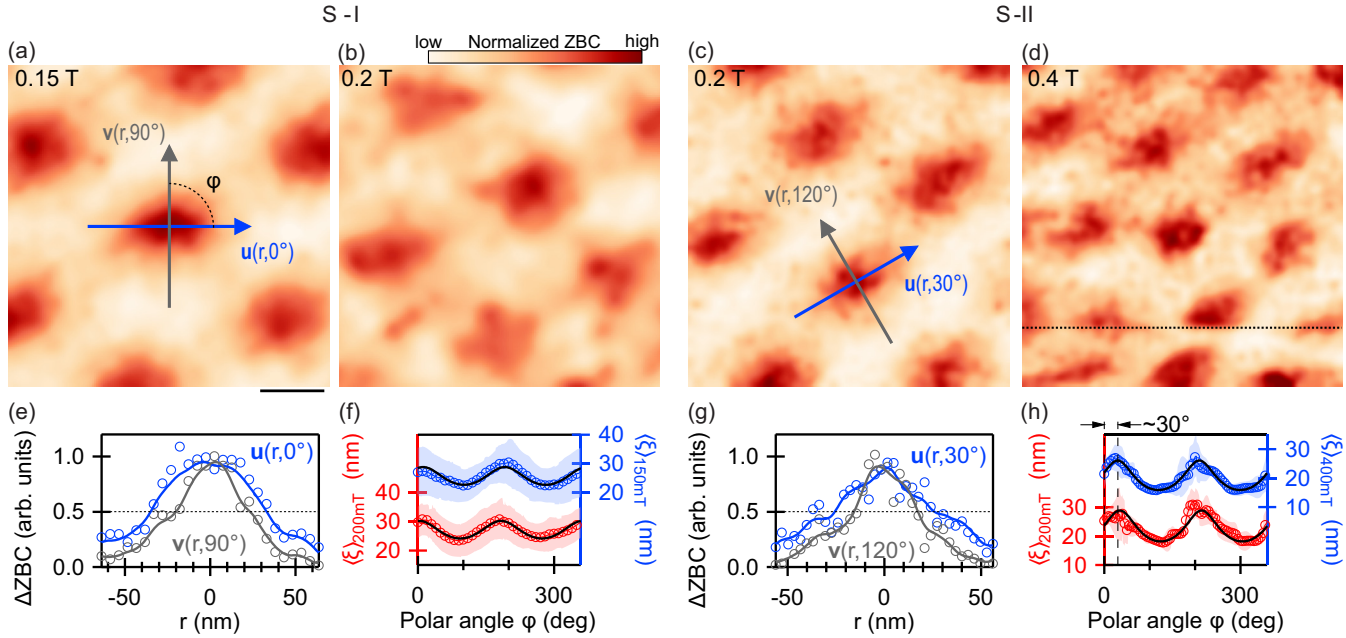

FIG. 1. Elongated vortices in CPSBS. [(a),(b)] Normalized zero-bias conductance (ZBC) maps taken on sample S-I in the out-of-plane magnetic field of 0.15 and 0.2 T. Stabilization parameters are $U = 5$ mV, $I = 200$ pA and $U_{\rm mod} = 100\ \mu V_{\rm p}$. [(c),(d)] Similar maps for sample S-II in 0.2 T and 0.4 T. Stabilization parameters are $U = 1$ mV, $I = 50$ pA, and $U_{\rm mod} = 100\ \mu V_{\rm p}$. Gaussian smoothing was applied to all maps to filter spatial variations of the ZBC smaller than the vortex size (unsmoothed data is shown in the SM [21]). The discontinuity [dotted line in (d)] is due to the vortex lattice motion during the measurement. [(e),(g)] Line profiles of the change in normalized ZBC (ΔZBC) taken across a vortex center along the vectors shown in (a) and (c); solid lines and open circles are smoothed and raw data, respectively. [(f),(h)] Angular dependence of the average vortex radius $\langle\xi\rangle$. Open circles denote the average of 53 (56) vortices measured for sample S-I at 0.15 T (0.2 T); for sample S-II, the average was from 6 (7) vortices at 0.2 T (0.4 T). The shaded area indicates the standard deviation and the solid-black line is a fit to the ellipse equation. The polar angle was measured from the horizontal axis, which is parallel to the monoclinic b axis.

calculations, which showed that the vortex anisotropy in a p-wave superconductor should rotate by 90° as a result of impurity scattering [20]. On a more disordered surface where the twofold lattice symmetry is smeared, we found that the vortex anisotropy axis is rotated by 30°, pointing to the rotation of the gap nodes/minima on the surface. Our symmetry analysis shows that rotation of the gap nodes is indeed possible in the presence of an emergent symmetry at the surface and, furthermore, the inversion symmetry breaking at the surface would lead to lifting of the nodes. The latter conclusion is consistent with the observed gap spectra. Our paper hence offers a framework to understand the intricate relation between crystal symmetry and the gap function in a topological superconductor.

II. RESULTS

A. Elongated vortices

We examine the SC gap structure on the surface of CPSBS by applying an out-of-plane magnetic field and imaging the vortex lattice of CPSBS in the mixed state. Even though a major portion of the cleaved surface of CPSBS does not show superconductivity, we were able to observe superconductivity on the sample surface at roughly 17% of the total scan area (see the Supplemental Material, SM [21] for details), which is slightly better than the case of $Cu_xBi_2Se_3$ [16]. Figures 1(a)-1(b) and 1(c)-1(d) show the spatially resolved normalized zero-bias conductance (ZBC) on the superconducting surface of CPSBS for two different samples, S-I and S-II, respectively, in various out-of-plane magnetic fields whose magnitude is indicated in each panel (additional data for other fields are shown within the SM [21]). A vortex lattice is clearly resolved, and the vortex density increases with increasing field. Importantly, all the observed vortices are deformed—the vortices in sample S-I are roughly elongated along the horizontal axis, while those in sample S-II are rotated by about 30° in comparison.

Naively, one would expect that elongated vortices reflect an anisotropy in the Ginzburg-Landau (GL) in-plane coherence length, which results from the SC gap anisotropy in k space, with the longest (shortest) coherence length associated with directions for which the gap value is the smallest (largest) [16]. However, it was recently pointed by theory that the local density of states (LDOS) around vortices imaged by STM experiments can acquire different geometries depending on the strength of impurity scattering [20]. In particular, it was shown that for a p-wave superconductor, the LDOS is elongated along the the direction perpendicular to the gap nodes, in contrast to the naive GL prediction for clean systems. We will discuss the relation between the vortex elongation and the gap nodes/minima in Sec. II C.

It is prudent to mention that a vortex-shape anisotropy can also be caused by a Fermi-velocity anisotropy [22,23]. However, the ARPES measurements on superconducting CPSBS [24] found no such anisotropy within the experimental error of ∼2%. Even if there were some unexpected Fermi-velocity

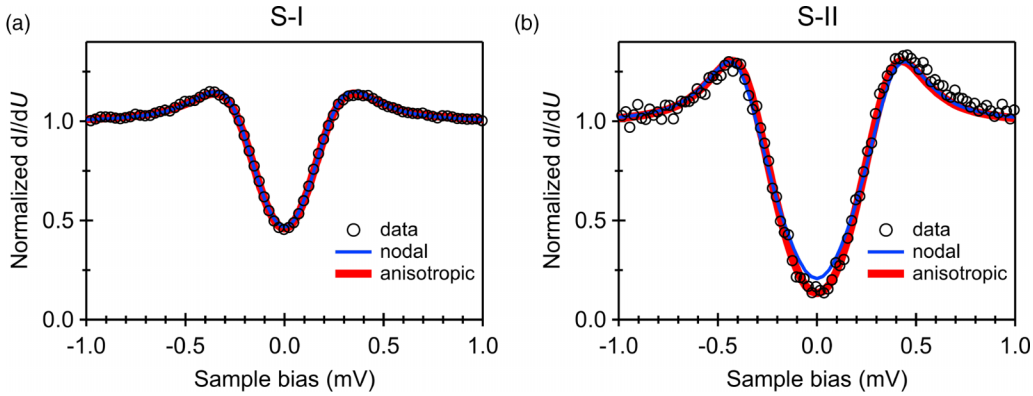

FIG. 2. Superconducting gap spectra. Representative high-resolution gap spectra taken in zero field, at the base temperature of 0.35 K and in the same area as the vortex maps. The spectrum in (a) is a result of averaging 10000 individual spectra covering an area of $(500\ \text{nm})^2$, while the data in (b) is after averaging 5000 individual spectra taken at the same spot to enhance the resolution. The fits of the data to Eq. (1) assuming two different gap functions [nodal (blue) and node-lifted anisotropic (red) types] are overlayed on the data. In these fits, the effective temperature was fixed at 0.7 K. The set of parameters (Δ_0, Δ_1, Γ) obtained from the fits in (a) for sample S-I are (0, 0.26, 0.03) and (0.07, 0.18, 0.05) for the nodal and node-lifted scenarios, respectively, and those for sample S-II in (b) are (0, 0.39, 0) and (0.11, 0.26, 0.01) for the two scenarios (all in mV unit). Any error of the fitting routine is well below the experimental uncertainty due to the spatial inhomogeneity of the total gap magnitude, which was about 0.05 meV in each area (see the SM [21]). Stabilization parameters are $U = 5$ mV, $I = 500$ pA for sample S-I (a) and $U = 3$ mV, $I = 50$ pA for sample S-II (b).

anisotropy in the region of the vortex lattice, we do not expect it can lead to an anisotropy of the vortex shape in the present case, because CPSBS is in the dirty limit (see the SM [21]) and a vortex-shape anisotropy cannot result purely from a Fermi-velocity anisotropy in the dirty limit [22]. Also, a vortex can appear elongated if the magnetic field is not perpendicular to the sample surface [25]; to dismiss this possibility, we intentionally tilted the applied magnetic field by about 10° both along the short and long vortex axes (see Fig. S9 within the SM [21]) and observed no significant change in the anisotropy. Hence, it can be concluded that the elongation of the vortex stems from the anisotropic gap.

To quantify the vortex elongation, we first determine the vortex lattice (see the SM [21] for details) and then take line-cuts of the ZBC at each lattice site corresponding to a vortex center. Examples of such line-cuts are shown in Figs. 1(e) and 1(g) for directions crossing the vortex shown in Figs. 1(a) and 1(c), respectively. We follow Sera *et al.* [20] to define the vortex-core radius ξ as the half width at half maximum, and determined it as a function of the polar angle φ. We obtained this $\xi(\varphi)$ for 53 (56) vortices in sample S-I at 0.15 T (0.2 T) and for 6 (7) vortices in sample S-II at 0.2 T (0.4 T). Note that ξ is not necessarily equal to the GL coherence length due to the scattering-induced LDOS [20]. The $\xi(\varphi)$ data are averaged over all vortices in each data set to yield $\langle\xi(\varphi)\rangle$, which is plotted for sample S-I in Fig. 1(f) and for sample S-II in Fig. 1(h). The observed φ dependence is reasonably well fit by the ellipse equation, and the fitting gives the ratio between the major and minor axes, $\gamma \equiv \langle\xi_{\text{major}}\rangle/\langle\xi_{\text{minor}}\rangle$, of ∼1.25 (∼1.55) for sample S-I (S-II). The fitting also gives the rotation angle of ∼30° for the vortices in sample S-II.

B. Superconducting gap spectra

As discussed above, our observation of elongated vortices points to an anisotropic SC gap. To investigate the anisotropy in the SC gap function, we analyzed the representative dI/dU spectra (Fig. 2) measured in zero field at the lowest fridge temperature of 0.35 K for samples S-I and S-II. We fit the spectra by using a generalization of Dynes formula [26] for the momentum-resolved superconducting DOS,

$$N_{\mathbf{k}}(E) = \left|\text{Re}\left[(E - i\Gamma)\Big/\sqrt{(E - i\Gamma)^2 - \Delta_{\mathbf{k}}^2}\right]\right|, \qquad (1)$$

where we assume a circular Fermi surface. Γ is an effective broadening parameter due to pair-breaking scattering and $\Delta_{\mathbf{k}}$ is the SC gap that can have a $\mathbf{k}$ dependence. We fit a twofold symmetric gap with $\Delta_{\mathbf{k}} = \Delta_0 + \Delta_1|\cos\theta_{\mathbf{k}}|$. When the gap is nodal, $\Delta_0 = 0$. The tunneling conductance dI/dU is given by

$$\frac{dI}{dU} \propto \int N_{\mathbf{k}}(E) f'(E + eU) d\mathbf{k} dE, \qquad (2)$$

where $f(E)$ is the Fermi-Dirac distribution function at the effective temperature T_{eff}. The effective temperature of our STM experiments at the fridge temperature of 0.35 K was independently determined by a measurement of pure Nb [27] to be 0.7 K, so we fixed $T_{\text{eff}} = 0.7$ K and used Γ, Δ_0, and Δ_1 as fitting parameters.

In Fig. 2, we show fits to two different types of gap function: (i) nodal gap ($\Delta_0 = 0$) and (ii) twofold symmetric gap with lifted nodes ($\Delta_0 \neq 0$). As is described in detail in the SM [21], the size of the SC gap on the CPSBS surface varies with location. Thanks to a relatively large local gap, the data in Fig. 2(b) from sample S-II have a low ZBC, which helps to infer if the nodes are lifted: The nodal fit of the spectrum yields a ZBC that is higher than the data even for $\Gamma = 0$, which is clearly unreasonable given the dirty-limit nature of CPSBS (see the SM [21]). On the other hand, a reasonable fit is obtained for the anisotropic gap with lifted nodes, yielding $\Delta_0 = 0.11$ meV and $\Delta_1 = 0.26$ meV with $\Gamma = 10$ μeV. Hence, the data in Fig. 2(b) strongly suggest that the nodes are lifted at the surface. Here we should note that the conclusion of lifted nodes is based on the fits to the commonly assumed sinusoidal gap function, and it may not be valid if the

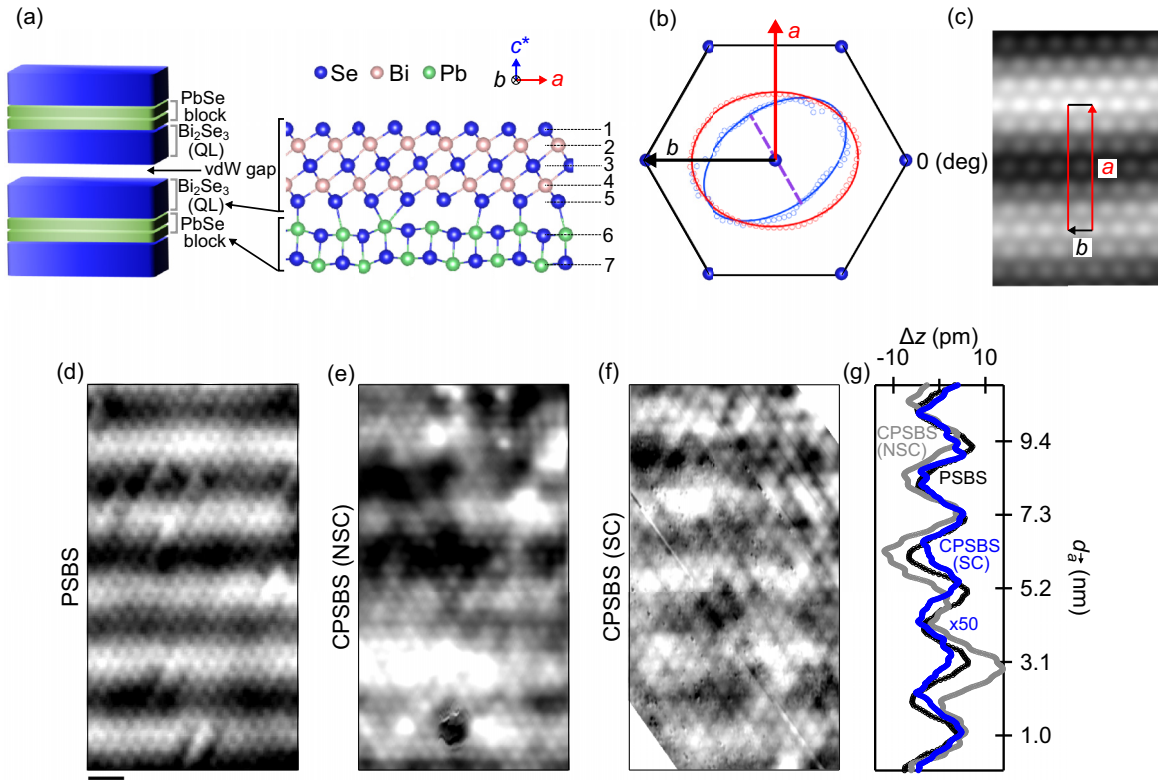

FIG. 3. Crystal structure and the gap anisotropy. (a) Schematics of the crystal structure of PSBS. (b) Average profile (open circles) and the fit to the ellipse equation (solid line) of vortices at 0.2 T for sample S-I (red) and S-II (blue) [the same data as in Figs. 1(f) and 1(h)] with respect to the top Se lattice and the monoclinic a and b axes; the mirror plane is parallel to a. (c) Fourier-filtered image of (d) overlayed with the monoclinic unit vectors; the stripe periodicity of ∼2.1 nm agrees with the a unit length. (d) Atomically resolved topmost Se layer on the cleaved surface of PSBS showing 1D stripes running across the whole surface. The stripe pattern is also observed on the nonsuperconducting areas of the CPSBS surface in sample S-II (e) and the superconducting area of sample S-I (f). Scale bar corresponds to 1 nm. (g) Averaged STM height profile along the vertical direction in (d) to (f). Scan parameters are $U = 900$ mV, $I = 20$ nA for (d); $U = 30$ mV, $I = 500$ pA for (e); and $U = 900$ mV, $I = 200$ pA for (f).

anisotropic gap has a non-sinusoidal function with unusually steep node. The large anisotropy ratio $(\Delta_0 + \Delta_1)/\Delta_0 \simeq 3.4$ implies a pronounced minima in the gap function, which is consistent with the finite quasiparticle scattering even in the absence of vortices. Due to a smaller local gap resulting in a large ZBC, the data in Fig. 2(a) from sample S-I do not allow us to distinguish between nodal and the node-lifted scenarios; nevertheless, the fit with the anisotropic gap function yields a reasonable result with an anisotropy ratio of ∼3.6. In fact, the spectra obtained at all the SC regions are consistent with the anisotropic gap function (see Fig. S11 within the SM [21]), even though the value of Δ_0 and Δ_1 varies significantly. This large variation appears to reflect the fact the the superconductivity in CPSBS (and in all other Bi_2Se_3-based superconductors) is weakened or disappear at a larger part of the surface, whose origin is a topic of on-going research: For example, in a recent paper [27] it was proposed that a strong electric field due to intrinsic surface band bending may break Cooper pairs near the surface. In the case of CPSBS, the strength of surface band bending would vary depending on the density of Cu dopants found on the surface.

To strengthen the conclusion of the anisotropic gap, we performed additional experiments on sample S-III to measure the dependence of the SC gap spectra on the direction of the in-plane magnetic field φ (see the SM [21] for details). The φ dependence of the spectra, in particular the conductance at zero bias, is clearly twofold symmetric (see Fig. S12 within the SM [21]). A similar phenomenon was reported for $Cu_xBi_2Se_3$ [16] and was taken as additional evidence for an anisotropic gap. These observations are also in good agreement with the theoretical prediction by Nagai [28], who showed that the angular dependence of the zero-energy density of states has deep minima when the in-plane magnetic field is aligned with the direction of the nodes in the Δ_4 gap realized in $Cu_xBi_2Se_3$.

C. Orientation of the gap minima

We now turn to the topographic images of CPSBS and those of pristine $(PbSe)_5(Bi_2Se_3)_6$ (called PSBS) to identify the orientation of the gap minima. Figure 3(a) shows the schematics of the crystal structure of PSBS/CPSBS. Upon cleaving the PSBS crystal, one usually obtains a surface that is terminated by a single quintuple layer (QL) of the Bi_2Se_3 unit on top of the PbSe layer [29]. Figure 3(d) shows a typical topograph on such a surface, where a clear one-dimensional (1D) stripe pattern with atomically resolved top Se layer is observed. Although the lattice in CPSBS is more disordered due to Cu intercalation, a similar stripe pattern is observed in atomic-resolution images on a SC area of CPSBS of sample

S-I [Fig. 3(f)] as well as on a nonsuperconducting (NSC) area of sample S-II [Fig. 3(e)]. The stripe corrugation is less pronounced in the SC area of sample S-I [Fig. 3(g)].

The 1D stripe can be understood as a commensuration effect (similar to a moiré pattern) arising from the stacking of the square PbSe lattice and the hexagonal Bi_2Se_3 lattice. One can see in Fig. 3(a) that the crystal structure repeats every six Se atoms in the layer 5 and every five Pb atoms in layer 6 along the a axis, and this repetition defines the unit length along the a axis. As shown in Fig. 3(c), the stripe periodicity agrees with the length of the monoclinic a axis, which clearly indicates that the stripes come from this commensuration of Se and Pb sublattices. This in turn allows for a unique determination of the in-plane monoclinic lattice vectors on the hexagonal top Se layer, i.e., the stripes are running along the b axis. While we were not able to resolve the crystal lattice in the SC area of sample S-II where the vortex lattice shown in Figs. 1(c) and 1(d) was recorded (a similar case was reported by Tao *et al.* [16] for $Cu_xBi_2Se_3$), we know from x-ray diffraction analysis that in our CPSBS sample the orientation of the monoclinic axes is macroscopically identical. This is further verified in STM since we only observed one fixed orientation of the 1D-stripe with respect to our scan coordinates, globally.

In Fig. 3(b), we replot the anisotropic ξ with respect to the hexagonal lattice and the monoclinic axes for both samples S-I and S-II. Focusing first on the data for S-I, it is to be remarked that the vortex core is elongated roughly along the monoclinic b axis, whereas the gap nodes in the bulk lie along the a axis [9]. This fact indicates that the vortex-shape anisotropy is not dictated by the GL coherence length anisotropy but by the maxima of the LDOS in the presence of impurity scattering. A recent theoretical study has reported that the maxima in the LDOS of a p-wave twofold-symmetric superconductor can be rotated by 90° in the presence of impurity scattering [20]. This result can be understood in terms of the quasiparticle trajectory picture obtained within the quasiclassical theory of superconductivity [30–32]. The LDOS at point $\mathbf{r}$ and energy ϵ for an isotropic two-dimensional Fermi surface can be generally evaluated as [33]

$$\mathrm{LDOS}(\mathbf{r},\epsilon) = -\nu(0)\int \frac{d\Omega_{\mathbf{k}}}{4\pi}\mathrm{Re}[\mathrm{tr}(\hat{g}^R(\mathbf{r},\tilde{\mathbf{k}},\epsilon))], \qquad (3)$$

where $\nu(0)$ is density of states at the Fermi energy and $\hat{g}^R(\mathbf{r},\tilde{\mathbf{k}},\epsilon)$ is the retarded Green's function obtained from the quasiclassical Eilenberger equation written as matrices in spin space, and $\tilde{\mathbf{k}} = \mathbf{k}/k_F$ is the momentum normalized by the Fermi momentum k_F. An analytic form for $\hat{g}^R(\mathbf{r},\tilde{\mathbf{k}},\epsilon)$ around a vortex core can be obtained by a convenient parametrization of the Green's functions that cast the Eilenberger equation in terms of matrix Ricatti equations. At low energies and near the vortex core, one can perform a Kramer-Pesch approximation, expanding the Green's function in ϵ/Δ_∞ and y/ξ_0, where Δ_∞ corresponds to the bulk gap, y is the quasiparticle trajectory impact parameter, ξ_0 is the superconducting coherence length $\xi_0 = v_F/(\pi\Delta_\infty)$, and v_F the Fermi velocity. Within this expansion, the Ricatti equations form a set of inhomogeneous linear differential equations with closed form solutions, from which it is possible to identify the condition for the divergence of the LDOS for an arbitrary anisotropic superconducting gap.

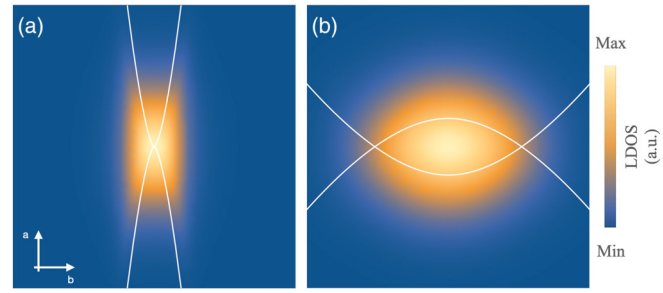

FIG. 4. LDOS from the quasiparticle trajectory picture. The enveloping curves of the quasiparticle paths at which the LDOS diverges are shown in white lines. The density plots correspond to the LDOS obtained by Green's functions with poles determined by the enveloping curves smeared by $\delta/\Delta_\infty = 0.05$ and with an isotropic exponential decay characterized by a length scale equal to $\xi_0/400$. Here Δ_∞ is the gap magnitude in the bulk, ϵ is the bias energy scale, and ξ_0 the coherence length. The field of view corresponds to $0.2\xi_0$ along the a and b directions. (a) Clean limit, with $\epsilon/\Delta_\infty = 10^{-4}$. (b) Dirty limit, with $\epsilon/\Delta_\infty = 0.02$.

This condition is given by a parametric equation in the in-plane angle θ around the vortex, which defines an enveloping function for quasiparticle paths given by

$$\begin{pmatrix} \frac{x}{\xi_0} \\ \frac{y}{\xi_0} \end{pmatrix} = \frac{\epsilon}{\Delta_\infty \lambda^2(\theta)} \begin{pmatrix} \frac{2}{\lambda(\theta)}\frac{\partial\lambda(\theta)}{\partial\theta}\cos\theta - \sin\theta \\ \frac{2}{\lambda(\theta)}\frac{\partial\lambda(\theta)}{\partial\theta}\sin\theta + \cos\theta \end{pmatrix}, \qquad (4)$$

where $\lambda(\mathbf{k}) = \sqrt{\frac{1}{2}\mathrm{tr}[\hat{\Delta}^\dagger(\mathbf{k})\hat{\Delta}(\mathbf{k})]}$, with $\hat{\Delta}(\mathbf{k})$ the superconducting order parameter matrix written in spin space. For a superconductor having a twofold-symmetric gap, the simplest form of gap anisotropy is captured by $\lambda(\theta) = \lambda_0|\cos\theta|$, with the corresponding envelope function and LDOS shown in Fig. 4. The LDOS is obtained from the poles determined by the enveloping function smeared by a small factor δ/Δ_∞ associated with the presence of phonons or impurity scattering. Note that in the dirty limit the anisotropy of the LDOS is rotated by 90° with respect to the anisotropy in the clean limit, the latter dictated by the coherence length anisotropy. For details, see [33]. A similar approach has been useful for understanding the rotation of vortices as a function of applied bias [34,35].

It is worthwhile to note that p-wave superconductivity is commonly known to be fragile against impurity scattering; however, in CPSBS the generalized Anderson theorem [11] protects the unconventional pairing even in the dirty limit. Note also that this impurity effect on the vortex shape was not considered in the previous study on $Cu_xBi_2Se_3$[16], which concluded that the gap minima at the surface are 90° rotated compared to the bulk.

Interestingly, the elongation axis of the vortices in sample S-II shown in Figs. 1(c) and 1(d) is 30° rotated from that in sample S-I. Following the conclusion that the vortex elongation occurs in the direction of gap maxima in CPSBS, the data in Figs. 1(c) and 1(d) suggest that on the SC surface of sample S-II, the gap minima are rotated from the monoclinic a axis by 30°, which is perpendicular to one of the mirror planes of D_{3d} symmetry and corresponds to the Δ_{4y} gap. In correspondence with this result, the in-plane magnetic-field-direction depen-

dence of the gap spectra observed on the surface of sample S-III, which was discussed in Sec. II B, also shows that the gap minima is rotated from the a axis by $\sim 20^\circ$ (see the SM [21] for details). As shown in Fig. S13 within the SM [21], the SC areas of both samples S-II and S-III are so disordered that the stripe pattern indicating the twofold symmetry of the lattice is no longer observed. This implies that the threefold symmetry of the Bi_2Se_3 QLs is effectively restored due to disorder in both samples. In the next section, we argue that the rotation of the gap minima observed on the SC surface of samples S-II and S-III can be understood as a consequence of this emergent symmetry.

III. THEORETICAL ANALYSIS

We now present a symmetry analysis, which provides a consistent picture for the above observations, under the assumption that the superconductivity observed on the surface inherits the unconventional pairing from the bulk. We emphasize that, although the nature of the superconductivity on the surface is apparently different from that of the bulk, it must be unconventional itself, because vortices cannot be anisotropic in the dirty limit of a conventional superconductor.

We start the discussion from the perspective of the Bi_2Se_3 QLs with D_{3d} point group symmetry. The minimal model for the normal state electronic structure that properly captures the topological properties of the bands is given in terms of two effective orbitals with opposite parity formed by a symmetric, labeled as 1, or antisymmetric 2, combination of p_z orbitals within the QLs [36,37]. In the orbital-spin basis $\Phi^\dagger_{\mathbf{k}} = (c^\dagger_{1\uparrow}, c^\dagger_{1\downarrow}, c^\dagger_{2\uparrow}, c^\dagger_{2\downarrow})_{\mathbf{k}}$, the normal-state Hamiltonian can be parametrized as

$$\hat{H}_0(\mathbf{k}) = \sum_{a,b} h_{ab}(\mathbf{k}) \hat{\tau}_a \otimes \hat{\sigma}_b, \tag{5}$$

where $\hat{\tau}_{a=1,2,3}$ are Pauli matrices encoding the orbital degrees of freedom (DOF), $\hat{\sigma}_{b=1,2,3}$ are Pauli matrices encoding the spin DOF, and $\hat{\tau}_0$ and $\hat{\sigma}_0$ are two-dimensional identity matrices in orbital and spin space, respectively. In the presence of time-reversal [acting as $\hat{\Theta} = K\hat{\tau}_0 \otimes (i\hat{\sigma}_2)$, where K stands for complex conjugation] and inversion (implemented as $\hat{P} = \hat{\tau}_3 \otimes \hat{\sigma}_0$) symmetries, the only allowed terms in the Hamiltonian have indices $(a, b) = \{(0, 0), (2, 0), (3, 0), (1, 1), (1, 2), (1, 3)\}$. The properties of the $\hat{\tau}_a \otimes \hat{\sigma}_b$ matrices under the point group operations allow us to associate each of these terms to a given irreducible representation (irrep) of D_{3d}, therefore constraining the momentum dependence of the form factors $h_{ab}(\mathbf{k})$ by symmetry. More details on the description of the normal state are given within the SM [21]. The important features to keep in mind are the following: (0,0) and (3,0) correspond to intra-orbital hopping, (2,0) corresponds to interorbital hopping, $(1, a)$, with $a = \{1, 2, 3\}$ correspond to spin-orbit coupling terms. In particular, (1,3) is associated with trigonal warping and is very small within the parameter range of validity of this effective model [37].

TABLE I. Classification of superconducting order parameters. Here we focus on momentum-independent SC order parameters in the microscopic basis for materials in the family of Bi_2Se_3. The $[a, b]$ indexes in the first column correspond to the parametrization of the SC gap function according to Eq. 6. The second to fifth columns give the irreducible representation associated with each order parameter for the cases of D_{3d}, D_{1d}, C_{1v}, and C_{3v} point group symmetry, respectively.

[a,b]	D_{3d}	D_{1d}	C_{1v}	C_{3v}
[0,0]	A_{1g}	A_{1g}	A_1	A_1
[3,0]				
[2,3]	A_{1u}	A_{1u}	A_2	A_2
[1,0]	A_{2u}	A_{2u}	A_1	A_1
[2,1]	E_u	A_{2u}	A_1	E
[2,2]		A_{1u}	A_2	

Following the parametrization of the normal state, the order parameters can be generally written as

$$\hat{\Delta}(\mathbf{k}) = \sum_{a,b} d_{ab}(\mathbf{k}) \hat{\tau}_a \otimes \hat{\sigma}_b (i\hat{\sigma}_2). \tag{6}$$

Focusing on local pairing mechanisms, the allowed momentum-independent gap matrices are associated with antisymmetric matrices $\hat{\tau}_a \otimes \hat{\sigma}_b(i\hat{\sigma}_2)$. These can be classified according to the irreps of the of D_{3d} point group, as displayed in the second column of Table I [13].

The QLs of Bi_2Se_3 have D_{3d} symmetry. In CPSBS, the presence of the PbSe layers reduces the point group symmetry from D_{3d} to D_{1d}, and the irreps are mapped according to the third column of Table I. The SC order parameter in the bulk of CPSBS is believed to be of the form [2,2], given its twofold symmetry and the presence of nodes along the mirror plane [9,11]. This is an odd-parity order parameter, which is interorbital and spin-triplet in nature. Note that, in the case of D_{1d} symmetry, this order parameter belongs to A_{1u} irrep. This is a one-dimensional irrep and the notion of nematicity does not apply as the threefold symmetry is explicitly broken by the lattice. Note, though, that the order parameter with indices [2,3] belongs to the same A_{1u} symmetry channel in D_{1d}. This means that an order parameter in A_{1u} is generally a linear superposition of [2,2] and [2,3]. Even if pairing is primarily driven by interactions promoting the order parameter [2,2], the combination of spin-orbit coupling terms (1,2) and (1,3) in the normal state Hamiltonian could lead to the development of SC correlations with [2,3] character. Nevertheless, as the trigonal warping term (1, 3) is small in the Bi_2Se_3 family of compounds [37], the corresponding mixing should also be small in the bulk of CPSBS, leading to a lifting of nodes that might be too small to be observed experimentally. This information is schematically conveyed in the second row of Fig. 5.

At the surface of CPSBS inversion symmetry is broken and the point group is reduced to C_{1v}. The irreps associated to the order parameters with momentum-independent gap matrices are mapped according to the fourth column of Table I. Now the order parameter [2,2] belongs to irrep A_2, and any order parameter in this symmetry channel should again be a linear

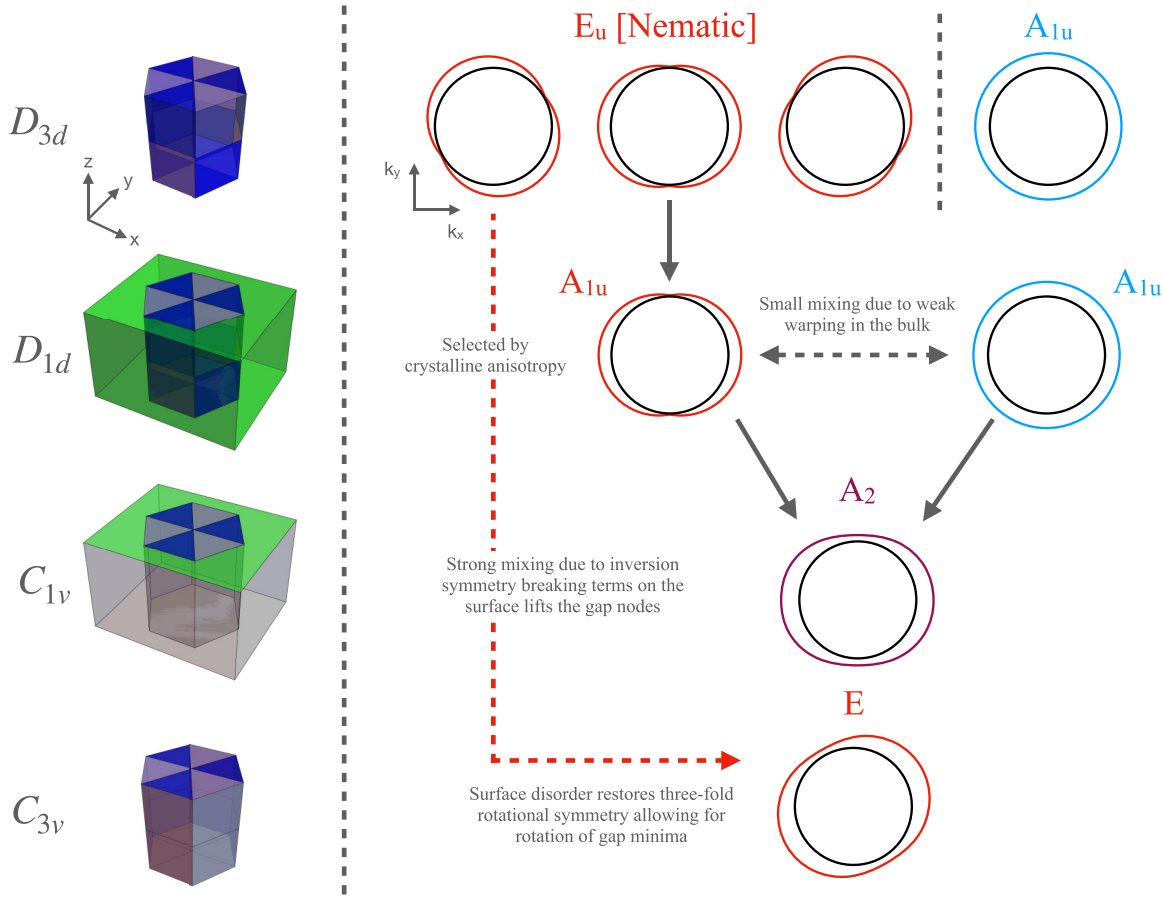

FIG. 5. Symmetry analysis of the superconducting order parameter. (Left) Representative objects following the same point group symmetries as Bi_2Se_3 (D_{3d}), CPSBS (D_{1d}), and the surface of CPSBS (C_{1v} or C_{3v}, without or with disorder, respectively). The color of the objects matches the corresponding Bi_2Se_3 and PbSe blocks in Fig. 3(a). (Right) SC gaps (colored lines) at the Fermi surfaces (black circles) for the symmetry channels relevant for the discussion in the text. More details on the parameters used to generate the figures for each symmetry scenario are given in the SM [21].

superposition of [2,2] and [2,3]. Note that due to inversion symmetry breaking at the surface, the normal-state Hamiltonian includes all (a, b) coefficients, allowing for multiple pairs of terms in the normal state to promote the mixing of the [2,2] and [2,3] order parameters (see detailed discussion in the SM [21]). These surface terms in the normal-state Hamiltonian contribute further to the lifting of gap nodes, as illustrated in the third row of Fig. 5, so that the node lifting at the surface would be stronger than that in the bulk. Here it should be emphasized that, as any gap in C_{1v} should still be symmetric or antisymmetric under reflections along the k_yk_z plane, the gap cannot be rotated under these symmetry considerations. For a rotation of gap nodes or gap minima to take place, a mixing of order parameters in different symmetry channels of C_{1v} would be required.

A possible origin of such a mixing is the strong disorder at the surface. The rotation of the gap minima was detected only in locations at which no stripe pattern could be observed by STM (see Fig. S13 within the SM [21]), suggesting that in these disordered areas the effect of the PbSe layers is weakened and the threefold rotational symmetry present in the Bi_2Se_3 layers is effectively restored. Under these considerations, the point group symmetry at the disordered surface can be identified as C_{3v}. Interestingly, this point group has a two-dimensional irrep labeled as E, which would allow for mixing of gaps [2,2] and [2,1] that are associated with different irreps in C_{1v}. Under the C_{3v} symmetry, by changing the mixing of these two order parameters in the absence of warping, we find that the gap minima can be tuned to any position along the circular Fermi surface. In particular, a ratio $d_{21}/d_{22} = 1$ generates minima at 30° from the bulk nodes. While the stability of this particular ratio requires an analysis of the energetics of the system, which is beyond the scope of this paper, the rotation by 30° corresponds to having the nodes along the a axis of the hexagonal notation [9] for D_{3d} symmetry. It is plausible that this ratio is in fact stable, as this is the direction of the nodes realized in $Cu_xBi_2Se_3$.

The last row of Fig. 5 schematically shows a gap that could be generated at the surface under these considerations. Here, it should be remarked that the two-component nature of the order parameter in the quintuple layers of Bi_2Se_3-based materials with D_{3d} symmetry is a necessary condition to explain the rotation of the gap at the surface of CPSBS. Therefore, the tunneling spectra and the vortex anisotropy observed in our experiment provide one more piece of evidence for the

intrinsically nematic nature of the SC gap in Bi_2Se_3-based materials.

IV. DISCUSSIONS AND CONCLUSIONS

We start our discussions by revisiting some of the experimental findings on $Cu_xBi_2Se_3$ samples. Some of the discrepancies between the bulk [4] and the surface [16] regarding the direction of the gap minima may be resolved by considering the effect of impurity scattering discussed in Sec. II C. However, in the literature, even in the bulk measurements on $Cu_xBi_2Se_3$, there are reports, which differ in the position of the gap minima with respect to the underlying lattice by 90° [3,4]. Recent Knight-shift measurements [17] ruled out a multidomain effect in the bulk of the sample, which was previously proposed [4] as the possible reason for the different orientations of the gap. It was proposed in [17] that the specific local environment in the sample caused by lattice distortion or strain from dopant intercalation and/or quenching (which is necessary for obtaining superconductivity) may be responsible for determining the nematic axis. A high-resolution x-ray diffraction (XRD) experiment on $Sr_xBi_2Se_3$ reported a tiny (∼0.02%) in-plane lattice distortion [38], while a multimodal synchrotron XRD experiment with a slightly lower resolution did not find any distortion [39]. Therefore, the situation in doped-Bi_2Se_3 superconductors is complicated and it is still unclear what dictates the orientation of the gap minima in them.

In contrast, the orientation of the gap minima in the bulk of CPSBS is robust due to the reduced symmetry of the crystal lattice, which has only one mirror plane, and the rotation of the gap minima observed here is a pronounced manifestation of the decisive role of crystalline symmetry in determining the anisotropic axis of the SC gap. The rotation of the gap minima also signifies the intrinsically nematic nature of the SC order parameter in Bi_2Se_3-based materials, which suggests that the pairing mechanism must be the same for all superconductors in this family of materials.

It is useful to mention that according to the theoretical calculations reported in [20], the effect of impurity scattering is different for *p*-wave and anisotropic *s*-wave order parameters even when the angular dependence of the gap magnitude $|\Delta_{\mathbf{k}}|$ is the same; in the latter case, there is no sign change in the anisotropic SC gap and the vortex shape becomes isotropic in the presence of strong scattering. Therefore, the observation of elongated vortices in the dirty limit gives additional evidence for the topological odd-parity gap function.

Given that the topological odd-parity superconductivity is realized in this family of superconductors, an important question is the observability of gapless Majorana surface states, the existence of which is guaranteed by topology. In the present case, the Majorana surface states are expected to comprise dispersive 2D gapless modes, and time-reversal symmetry dictates that they have a helical spin-momentum locking [1]. The experimental difficulty in observing such Majorana surface states in this family of materials comes from the quasi-2D nature of the Fermi surface [1] and the destruction of superconductivity at a major portion of the surface [16,27,40]. The former implies that the Majorana surface states do not appear on the top surface, and the latter implies that the area where the superconductivity reaches the surface is surrounded by nonsuperconducting areas, causing the possible Majorana states (which may appear at the boundary) to merge with the surrounding metallic states, such that little spectral feature can be observed via STM.

In this connection, it is worthwhile to mention that a peculiar zero-bias conductance peak (ZBCP) has been observed in point-contact spectroscopy on $Cu_xBi_2Se_3$ [41–43] and on $Nb_xBi_2Se_3$ [44]. While there is an argument [43] that the ZBCP is simply due to Andreev reflections expected from the Blonder-Tinkham-Klapwijk (BTK) theory [45] for a high transparency contact, it was pointed out that the conductance dip, which is consistently observed at the superconducting gap energy, is incompatible with the BTK theory and points to *p*-wave pairing [44]. It is useful to note that those point-contact spectroscopy experiments had no problem in detecting superconductivity at the surface, which suggests that the mesoscopic metal in contact with the surface plays a role in locally restoring the superconductivity beneath the contact (via, e.g., electron transfer). One may further speculate that such a mesoscopic metal accesses the boundary of the locally restored superconductivity. Hence, well-controlled point-contact spectroscopy experiments might be a viable way to address the Majorana surface states expected for this family of superconductors.

The present result of our STM experiments on CPSBS, taken together with the complications in the orientation of the gap minima in $Cu_xBi_2Se_3$, clearly shows that the odd-parity gap function is highly sensitive to crystal symmetry in the topological superconductors derived from Bi_2Se_3. The symmetry-based analysis of the possible superpositions of different gap functions presented here gives a useful framework to understand odd-parity topological superconductors.

Raw data used in the generation of main and supplementary figures are available in Zenodo [46].

ACKNOWLEDGMENTS

This project has received funding from the European Research Council (ERC) under the European Union's Horizon 2020 research and innovation programme (Grant Agreement No. 741121) and was also funded by the Deutsche Forschungsgemeinschaft (DFG, German Research Foundation) under CRC 1238 - 277146847 (Subprojects A04 and B06) as well as under Germany's Excellence Strategy - Cluster of Excellence Matter and Light for Quantum Computing (ML4Q) EXC 2004/1 - 390534769. A.R. is supported by the Swiss National Science Foundation through the Ambizione Grant No. 186043.

APPENDIX

Material. We grew $(PbSe)_5(Bi_2Se_3)_6$ single crystals using a modified Bridgeman method as described previously [9,18]. Cu was electrochemically intercalated using the recipe of Kriener *et al.* [47] with a nominal *x* value of 1.36. The SC shielding fraction of the resulting CPSBS sample was measured using a Quantum Design superconducting quantum interference device (SQUID) magnetometer (see Fig. S1

within the SM [21]) and was 59% for sample S-I and 61% for sample S-II.

STM experiments. STM experiments were carried out under UHV conditions with a commercial system (Unisoku USM1300) operating at 0.35 K. STM images were recorded in the constant-current mode at the set current I and sample bias voltage U. dI/dU curves and dI/dU maps were obtained either using a lock-in amplifier by modulating U_{bias} and demodulating I, or by recording a series of I-U curves followed by numerical differentiation. The dI/dU maps displayed in Fig. 1 were smoothed by using a standard Gaussian filter with the smallest (3×3 points) kernel, corresponding to 15×15 nm^2 (a), 20×20 nm^2 (b), and 9.35×9.35 nm^2 (c),(d), with up to three iterations. The dI/dU spectra displayed in Fig. 2 were obtained by taking the numerical derivative of raw I-U data and subsequently applying a simple low-pass filter (binominal 21 passes). All STM data were analyzed using Igor Pro 9. We used in-house electrochemically etched W tips, first prepared on the Cu(111) crystal. Tip forming is done until a clean signature of the surface state is observed in spectroscopy. Prior to STM measurements, the crystals were cleaved under UHV conditions as described in [27].

[1] M. Sato and Y. Ando, Topological superconductors: A review, Rep. Prog. Phys. **80**, 076501 (2017).

[2] S. Yonezawa, Nematic superconductivity in doped Bi_2Se_3 topological superconductors, Condens. Matter **4**, 2 (2019).

[3] K. Matano, M. Kriener, K. Segawa, Y. Ando, and G.-q. Zheng, Spin-rotation symmetry breaking in the superconducting state of $Cu_xBi_2Se_3$, Nat. Phys. **12**, 852 (2016).

[4] S. Yonezawa, K. Tajiri, S. Nakata, Y. Nagai, Z. Wang, K. Segawa, Y. Ando, and Y. Maeno, Thermodynamic evidence for nematic superconductivity in $Cu_xBi_2Se_3$, Nat. Phys. **13**, 123 (2017).

[5] Z. Liu, X. Yao, J. Shao, M. Zuo, L. Pi, S. Tan, C. Zhang, and Y. Zhang, Superconductivity with topological surface state in $Sr_xBi_2Se_3$, J. Am. Chem. Soc. **137**, 10512 (2015).

[6] Y. Pan, A. M. Nikitin, G. K. Araizi, Y. K. Huang, Y. Matsushita, T. Naka, and A. de Visser, Rotational symmetry breaking in the topological superconductor $Sr_xBi_2Se_3$ probed by upper-critical field experiments, Sci. Rep. **6**, 28632 (2016).

[7] J. Shen, W.-Y. He, N. F. Q. Yuan, Z. Huang, C.-w. Cho, S. H. Lee, Y. S. Hor, K. T. Law, and R. Lortz, Nematic topological superconducting phase in Nb-doped Bi_2Se_3, npj Quantum Mater. **2**, 59 (2017).

[8] T. Asaba, B. J. Lawson, C. Tinsman, L. Chen, P. Corbae, G. Li, Y. Qiu, Y. S. Hor, L. Fu, and L. Li, Rotational symmetry breaking in a trigonal superconductor Nb-doped Bi_2Se_3, Phys. Rev. X **7**, 011009 (2017).

[9] L. Andersen, Z. Wang, T. Lorenz, and Y. Ando, Nematic superconductivity in $Cu_{1.5}(PbSe)_5(Bi_2Se_3)_6$, Phys. Rev. B **98**, 220512(R) (2018).

[10] M. S. Scheurer, M. Hoyer, and J. Schmalian, Pair breaking in multiorbital superconductors: An application to oxide interfaces, Phys. Rev. B **92**, 014518 (2015).

[11] L. Andersen, A. Ramires, Z. Wang, T. Lorenz, and Y. Ando, Generalized Anderson's theorem for superconductors derived from topological insulators, Sci. Adv. **6**, eaay6502 (2020).

[12] B. Zinkl and A. Ramires, Sensitivity of superconducting states to the impurity location in layered materials, Phys. Rev. B **106**, 014515 (2022).

[13] L. Fu and E. Berg, Odd-parity topological superconductors: Theory and application to $Cu_xBi_2Se_3$, Phys. Rev. Lett. **105**, 097001 (2010).

[14] L. Fu, Odd-parity topological superconductor with nematic order: Application to $Cu_xBi_2Se_3$, Phys. Rev. B **90**, 100509(R) (2014).

[15] I. Kostylev, S. Yonezawa, Z. Wang, Y. Ando, and Y. Maeno, Uniaxial-strain control of nematic superconductivity in $Sr_xBi_2Se_3$, Nat. Commun. **11**, 4152 (2020).

[16] R. Tao, Y.-J. Yan, X. Liu, Z.-W. Wang, Y. Ando, Q.-H. Wang, T. Zhang, and D.-L. Feng, Direct visualization of the nematic superconductivity in $Cu_xBi_2Se_3$, Phys. Rev. X **8**, 041024 (2018).

[17] T. Kawai, C. G. Wang, Y. Kandori, Y. Honoki, K. Matano, T. Kambe, and G.-q. Zheng, Direction and symmetry transition of the vector order parameter in topological superconductors $Cu_xBi_2Se_3$, Nat. Commun. **11**, 235 (2020).

[18] S. Sasaki, K. Segawa, and Y. Ando, Superconductor derived from a topological insulator heterostructure, Phys. Rev. B **90**, 220504(R) (2014).

[19] Y. Ando and L. Fu, Topological crystalline insulators and topological superconductors: From concepts to materials, Annu. Rev. Condens. Matter Phys. **6**, 361 (2015).

[20] Y. Sera, T. Ueda, H. Adachi, and M. Ichioka, Relation of superconducting pairing symmetry and non-magnetic impurity effects in vortex states, Symmetry **12**, 175 (2020).

[21] See Supplemental Material at http://link.aps.org/supplemental/10.1103/PhysRevB.109.104507 for additional data and discussions, which includes Refs. [48–51].

[22] A. Odobesko, F. Friedrich, S.-B. Zhang, S. Haldar, S. Heinze, B. Trauzettel, and M. Bode, Anisotropic vortices on superconducting Nb(110), Phys. Rev. B **102**, 174502 (2020).

[23] H. Kim, Y. Nagai, L. Rózsa, D. Schreyer, and R. Wiesendanger, Anisotropic non-split zero-energy vortex bound states in a conventional superconductor, Appl. Phys. Rev. **8**, 031417 (2021).

[24] K. Nakayama, H. Kimizuka, Y. Tanaka, T. Sato, S. Souma, T. Takahashi, S. Sasaki, K. Segawa, and Y. Ando, Observation of two-dimensional bulk electronic states in the superconducting topological insulator heterostructure $Cu_x(PbSe)_5(Bi_2Se_3)_6$: Implications for unconventional superconductivity, Phys. Rev. B **92**, 100508(R) (2015).

[25] J. A. Galvis, E. Herrera, C. Berthod, S. Vieira, I. Guillamón, and H. Suderow, Tilted vortex cores and superconducting gap anisotropy in 2H-$NbSe_2$, Commun. Phys. **1**, 30 (2018).

[26] R. C. Dynes, V. Narayanamurti, and J. P. Garno, Direct measurement of quasiparticle-lifetime broadening in a strong-coupled superconductor, Phys. Rev. Lett. **41**, 1509 (1978).

[27] M. Bagchi, J. Brede, and Y. Ando, Observability of superconductivity in Sr-doped Bi_2Se_3 at the surface using scanning tunneling microscope, Phys. Rev. Mater. **6**, 034201 (2022).

[28] Y. Nagai, Field-angle-dependent low-energy excitations around a vortex in the superconducting topological insulator $Cu_xBi_2Se_3$, J. Phys. Soc. Jpn. **83**, 063705 (2014).

[29] K. Nakayama, S. Souma, C. X. Trang, D. Takane, C. Chen, J. Avila, T. Takahashi, S. Sasaki, K. Segawa, M. C. Asensio *et al.*, Nanomosaic of topological Dirac states on the surface of $Pb_5Bi_{24}Se_{41}$ observed by nano-ARPES, Nano Lett. **19**, 3737 (2019).

[30] G. Eilenberger, Transformation of Gorkov's equation for type II superconductors into transport-like equations, Z. Phys. A: Hadrons Nucl. **214**, 195 (1968).

[31] T. Kita, Gor'kov, Eilenberger, and Ginzburg–Landau equations, *Statistical Mechanics of Superconductivity* (Springer Japan, Tokyo, 2015), pp. 201–227.

[32] N. Kopnin, *Theory of Nonequilibrium Superconductivity* (Oxford University Press, Oxford, 2001).

[33] Y. Nagai, Y. Ueno, Y. Kato, and N. Hayashi, Analytical formulation of the local density of states around a vortex core in unconventional superconductors, J. Phys. Soc. Jpn. **75**, 104701 (2006).

[34] M. Ichioka, N. Hayashi, N. Enomoto, and K. Machida, Vortex structure in d-wave superconductors, Phys. Rev. B **53**, 15316 (1996).

[35] S.-i. Kaneko, K. Matsuba, M. Hafiz, K. Yamasaki, E. Kakizaki, N. Nishida, H. Takeya, K. Hirata, T. Kawakami, T. Mizushima, and K. Machida, Quantum limiting behaviors of a vortex core in an anisotropic gap superconductor, J. Phys. Soc. Jpn. **81**, 063701 (2012).

[36] H. Zhang, C.-X. Liu, X.-L. Qi, X. Dai, Z. Fang, and S.-C. Zhang, Topological insulators in Bi_2Se_3, Bi_2Te_3 and Sb_2Te_3 with a single Dirac cone on the surface, Nat. Phys. **5**, 438 (2009).

[37] C.-X. Liu, X.-L. Qi, H. J. Zhang, X. Dai, Z. Fang, and S.-C. Zhang, Model Hamiltonian for topological insulators, Phys. Rev. B **82**, 045122 (2010).

[38] A. Y. Kuntsevich, M. A. Bryzgalov, V. A. Prudkoglyad, V. P. Martovitskii, Y. G. Selivanov, and E. G. Chizhevskii, Structural distortion behind the nematic superconductivity in $Sr_xBi_2Se_3$, New J. Phys. **20**, 103022 (2018).

[39] M. P. Smylie, Z. Islam, G. D. Gu, J. Schneeloch, R. D. Zhong, S. Rosenkranz, W. K. Kwok, and U. Welp, Multimodal synchrotron x-ray diffraction across the superconducting transition of $Sr_{0.1}Bi_2Se_3$, arXiv:2207.13221.

[40] N. Levy, T. Zhang, J. Ha, F. Sharifi, A. A. Talin, Y. Kuk, and J. A. Stroscio, Experimental evidence for s-wave pairing symmetry in superconducting $Cu_xBi_2Se_3$ single crystals using a scanning tunneling microscope, Phys. Rev. Lett. **110**, 117001 (2013).

[41] S. Sasaki, M. Kriener, K. Segawa, K. Yada, Y. Tanaka, M. Sato, and Y. Ando, Topological superconductivity in $Cu_xBi_2Se_3$, Phys. Rev. Lett. **107**, 217001 (2011).

[42] T. Kirzhner, E. Lahoud, K. B. Chaska, Z. Salman, and A. Kanigel, Point-contact spectroscopy of $Cu_{0.2}Bi_2Se_3$ single crystals, Phys. Rev. B **86**, 064517 (2012).

[43] H. Peng, D. De, B. Lv, F. Wei, and C.-W. Chu, Absence of zero-energy surface bound states in $Cu_xBi_2Se_3$ studied via Andreev reflection spectroscopy, Phys. Rev. B **88**, 024515 (2013).

[44] C. Kurter, A. D. K. Finck, E. D. Huemiller, J. Medvedeva, A. Weis, J. M. Atkinson, Y. Qiu, L. Shen, S. H. Lee, T. Vojta, P. Ghaemi, Y. S. Hor, and D. J. Van Harlingen, Conductance spectroscopy of exfoliated thin flakes of $Nb_xBi_2Se_3$, Nano Lett. **19**, 38 (2019).

[45] G. E. Blonder, M. Tinkham, and T. M. Klapwijk, Transition from metallic to tunneling regimes in superconducting microconstrictions: Excess current, charge imbalance, and supercurrent conversion, Phys. Rev. B **25**, 4515 (1982).

[46] M. Bagchi, J. Brede, A. Ramires, and Y. Ando, Zenodo, https://doi.org/10.5281/zenodo.10684776 (2024).

[47] M. Kriener, K. Segawa, Z. Ren, S. Sasaki, S. Wada, S. Kuwabata, and Y. Ando, Electrochemical synthesis and superconducting phase diagram of $Cu_xBi_2Se_3$, Phys. Rev. B **84**, 054513 (2011).

[48] M. R. Eskildsen, M. Kugler, S. Tanaka, J. Jun, S. M. Kazakov, J. Karpinski, and Ø. Fischer, Vortex imaging in the π band of magnesium diboride, Phys. Rev. Lett. **89**, 187003 (2002).

[49] N. Bergeal, V. Dubost, Y. Noat, W. Sacks, D. Roditchev, N. Emery, C. Hérold, J.-F. Marêché, P. Lagrange, and G. Loupias, Scanning tunneling spectroscopy on the novel superconductor CaC_6, Phys. Rev. Lett. **97**, 077003 (2006).

[50] C. Renner, A. D. Kent, P. Niedermann, O. Fischer, and F. Lévy, Scanning tunneling spectroscopy of a vortex core from the clean to the dirty limit, Phys. Rev. Lett. **67**, 1650 (1991).

[51] K. Nakayama, K. Eto, Y. Tanaka, T. Sato, S. Souma, T. Takahashi, K. Segawa, and Y. Ando, Manipulation of topological states and the bulk band gap using natural heterostructures of a topological insulator, Phys. Rev. Lett. **109**, 236804 (2012).